Applications in Engineering Science 20 (2024) 100200

Contents lists available at ScienceDirect

Applications in Engineering Science

journal homepage: www.sciencedirect.com/journal/applications-in-engineering-science

A filter calibration method for laser-scanned weld toe geometries

Finn Renken [a,*], Matthias Jung [c], Sören Ehlers [b], Moritz Braun [b]

[a] Institute for Ship Structural Design and Analysis, Hamburg University of Technology, Am Schwarzenberg Campus 4 C, Hamburg 21073, Germany
[b] German Aerospace Center (DLR), Institute of Maritime Energy Systems, Geesthacht, Germany
[c] Fraunhofer Institute for Mechanics of Materials IWM, Freiburg, Germany

ARTICLE INFO

Keywords:
Weld toe measurement
Laser scanning
Filter calibration
Data smoothing
Universal filter

ABSTRACT

The scanning of weld seams can be used to evaluate the local weld toe geometry for fatigue assessments. Laser scanned weld seam profiles often contain noise which complicates the accurate measurement of the weld toe geometry. For that reason, filtering of the scanned data is necessary. The issue at hand is that a filtering method can significantly affect the measurement results. Therefore, a calibration of the filter input parameters is needed. In this study, a calibration method for filtered laser-scanned weld profiles is presented by using artificial weld toe geometries. The adjustment of different filter functions is achieved by using an optimization method on predefined weld toes with an artificial noise. The resulting input data for the filter functions is tested on a real specimen to verify the method. Through the calibration method it is possible to achieve satisfactory measurement results with precisely set input parameters for the filter functions. The most suitable filter functions for the measurement of the weld toe are the Gaussian and the Lowpass filter. Both functions are adequate as a universally applicable filter. For the evaluation of the measurement results of the radii and angles, a tolerance range is introduced, which is defined by the theoretically minimum measurable radii and angles. Using an adjusted Lowpass filter and a point distance of 0.07 mm set by the laser scanner, a measurement within the tolerance range of 0.2 mm is achievable for the weld toe radius. For the weld toe angle, the tolerance range of 1.5° is achieved for the majority of measurements.

Nomenclature

Variable	Meaning	Unit
α	Weld toe angle	°
c_1	Cognitive coefficient	–
c_2	Social coefficient	–
i	Particle index	–
$gbest$	Best position of the swarm	–
P	Number of particles	–
$pbest$	Best position of a particle	–
R	Weld toe radius	mm
r_1	Random number between 0 and 1	–
r_2	Random number between 0 and 1	–
s	Point distance	mm
t	Iteration step	–
V	Velocity of a particle	–
w	Inertia	–
WT	Weld toe	–
X	Position of a particle	–
x	x-coordinate	mm
y	y-coordinate	mm

1. Introduction

Engineering structures are susceptible to fatigue failure due to the local weld geometry, which in this case acts as a notch (Zerbst et al., 2017; Alam et al., 2010). This notch effect is particularly important for high-strength steels and influences the fatigue strength (Ottersböck et al., 2016; Shiozaki et al., 2018). Especially the geometry of the weld toe, which includes its radius and angle, is of interest here (Lee et al., 2009; Braun and Kellner, 2022). These two parameters are relevant with regard to fatigue strength and can significantly change the service life of a weld (Schork et al., 2020; Harati et al., 2015). For that reason post weld treatments like hammer peening are used to modify the weld toe geometry for better fatigue behavior (Fricke, 2015). A larger weld toe radius for example can increase the fatigue strength (Tsang et al., 2018). On the other hand, corrosion in conjunction with the weld seam geometry, can result in poorer fatigue strength (Shojai et al., 2024). The weld toe parameters are also an indicator of the weld quality (Welding - Fusion-welded joints in steel, 2014). Therefore, the knowledge of the

* Corresponding author.
E-mail address: finn.renken@tuhh.de (F. Renken).

https://doi.org/10.1016/j.apples.2024.100200
Received 1 June 2024; Received in revised form 1 October 2024; Accepted 5 November 2024
Available online 6 November 2024

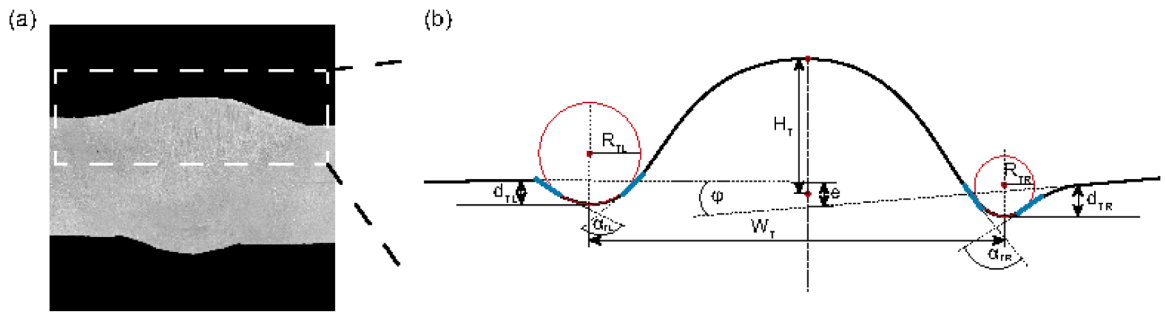

Fig. 1. Definition of the weld toe radius and weld toe angle of a butt weld based on Braun et al. (2022b).

weld toe parameters is important to assess the fatigue behavior or the quality of a weldment. Various methods are available to measure the weld toe parameters. It is possible to use manual measuring methods by means of test gauges, measuring micrographs on the computer or complete computer-aided evaluation methods, which, for example, evaluate laser-scanned weld surfaces (Stenberg et al., 2017; HOU, 2007; Niederwanger et al., 2020; Cho et al., 2022). A comparison of different measurement methods is presented in Schubnell et al. (2020). Most computer-aided methods use 2D sections which are generated from a point cloud which can be seen in Niraula et al. (2023) and Hultgren et al. (2021). These cross sections of the weld seam can be evaluated automatically. The results are reproducible due to a stored algorithm. In addition, this method is many-times faster than manual measurement methods. The weld toe parameters, such as the weld toe radius, usually require an accuracy of a tenth of a millimeter to be defined sufficiently (Braun et al., 2022a). Therefore, an accurate resolution is necessary. However, the measured surface point cloud is often affected by noise, making an accurate measurement impossible (Amir and Thörnberg, 2017; Kažukauskas et al., 2023; Cho et al., 2022). Thus, the 2D sections must be smoothed using a filter (Schubnell et al., 2020). In Rohani Raftar et al. (2024) a Gauss Filter was used for that purpose. However, these filter methods strongly affect the results and the influence needs to be examined. To ensure that the actual weld toe geometry is correctly mapped an adjustment of the filter input parameters is necessary. With a well-adjusted filter, the noise of the input data can be removed and a more accurate measurement of the weld toes is possible. Therefore, a filtering method must be determined that can produce an accurate image.

In this study, a suitable filter calibration method for filtered laser-scanned 2D weld seam sections is identified. For this purpose, automatically-generated initial weld profiles with specified weld toe parameters were created. To represent a real specimen a predefined noise will be added to the initial geometry to emulate the noise in the real-world measurement process. The noise of the sensor system can be analyzed by evaluating the even areas of a real specimen. These weld profiles are measured by means of a computer-aided evaluation with different filter functions. To assess the accuracy of the measurement the results can be compared to the initial geometry. The aim is to find a filter that can be used universally for a wide range of different weld toe geometries. Such a universal filter should work with fixed predefined parameters for common weld toes geometries in combination with the same laser scanner. The purpose is to generate an approximation of the weld toe that is as accurate as possible.

2. Measurement method

For the measurements of the weld toe parameters a computer-aided measurement method is used which can detect and measure the weld toes automatically. The 2D cross sections of the weld are mathematically described by a cubic parametric spline. More details of this method can be found in Renken et al. (2021). The measurement method is updated by enabling different filter methods and is ported to Python. Relevant weld toe parameters in this study are the weld toe radius and angle. The definition is shown in Fig. 1 where R describes the weld toe radius and α the weld toe angle. Other parameters like the undercut (d_T), weld reinforcement (H_T) and angular misalignment (ϕ) will not be evaluated in this study.

2.1. Weld toe radius

For the weld toe radius, the cubic parametric spline is evaluated at a given position with the following formula (Merziger, 2013),

$$R = \left| \frac{\left(1 + \left(\frac{\delta y}{\delta x}\right)^2\right)}{\frac{\delta^2 y}{\delta x^2}} \right|^{\frac{3}{2}} \tag{2.1}$$

where R describes the radius, and x and y are the coordinates of the weld profile.

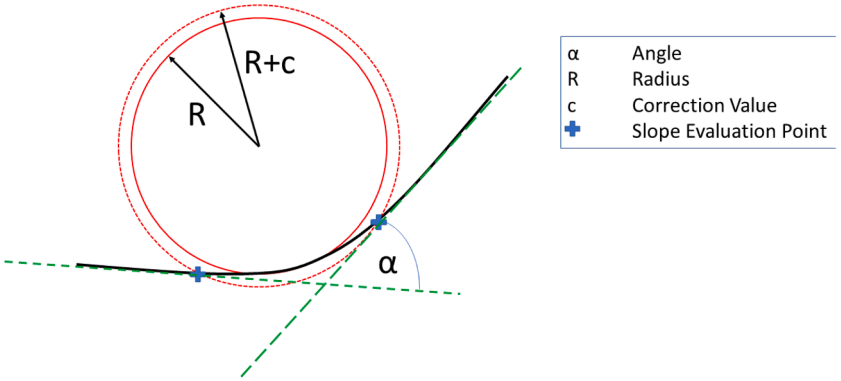

Fig. 2. Weld toe angle measurement with a correction value.

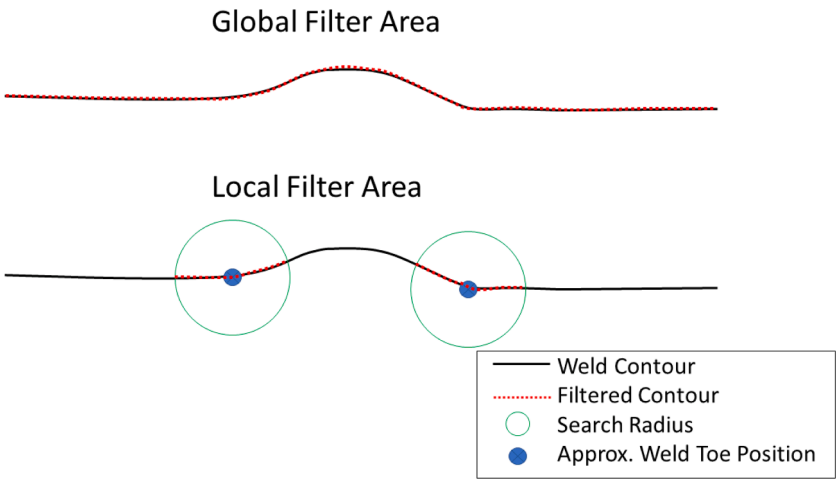

Fig. 3. Different filter areas.

2.2. Weld toe angle

The weld toe angle is determined using the circle of curvature. At each point the circle of curvature is formed and the contour of the weld slice is evaluated. The two points at which the weld contour no longer follows the circle of curvature is defined as an evaluation point for the weld toe angle. For these points, the slope of the cubic parametric spline is determined. With the slope two linear lines can be fitted. The angle of intersection between these lines defines the angle. To prevent that both evaluation points are at the same location, a correction value is introduced which increases the curvature circle by a predefined value (see Fig. 2). This value has an effect on the measurement accuracy due to the fact that the slope evaluation points affect the result of the weld toe angle. A suitable value for the correction value is determined in the course of this study.

2.3. Identification of the weld toe

Before the filtering, the weld toes must be identified. The weld toe needs a mathematical description. It is possible to use the smallest radius or the largest curvature for the identification of the weld toe (Schubnell et al., 2020; Ottersböck et al., 2021). However, this approach is highly susceptible to local irregularities in the scan and completely neglects the angle, which also has a strong influence (Randić et al., 2019; Schork et al., 2020, 2018; Schubnell et al., 2024). For this reason, a combination of the radius and the angle will be used. The radius and the angle will be calculated at each point of the weld toe area. In principle, it can be said that a notch is the worst where the radius is small and the angle is large. Thus, following definition is used for the weld toe WT,

$$WT = \max\left(\frac{\alpha}{R}\right) \tag{2.2}$$

where α describes the weld toe angle and R describes the weld toe radius. The maximum value along the weld toe area defines the weld toe.

2.4. Filter areas

For the evaluation, two filter areas are used. A distinction is made between a global and a local filter area. The global filter smoothens the complete weld geometry with the selected filter function and searches the weld toes. The global approach is less susceptible to smaller irregularities and does not require a search radius for filtering. As the global filter is applied to the entire slice, the filter must be set more precisely so that the weld toe is not distorted too much. With the local filter area, the approximate position of the weld toe is identified. At that position, a local filtering of the area will be performed. That requires a search radius which defines the filter areas. The local approach allows a closer look at the weld toe, but is more easily influenced by minor irregularities. The two different filter areas are shown in Fig. 3.

Table 1
Different filter functions with their input parameters.

Dimension	Filter Function	Parameter	
One-dimensional	Gaussian	Standard deviation σ	
	Lowess	Fraction of the data	
	Moving Average	Window length	
	Polynomial	Polynomial degree	
Two-dimensional	B-Spline	Number of nodes	Degree of the spline
	Lowpass	Cut-off frequency	Degree of the filter
	Savitzky-Golay	Window length	Polynomial degree

2.5. Filter functions

For the evaluation, several filter functions are tested with the two filter areas. The following filter functions are considered:

- B-Spline
- Gaussian
- Lowess
- Lowpass
- Moving Average
- Polynomial
- Savitzky-Golay

A distinction is made between one-parameter and two-parameter filters. The parameters can be seen in Table 1.

3. Experimental procedure

To test the filters, test slices must be generated with known weld toe geometry. This is only possible using automatically-generated sections with predefined geometry. A predefined noise must be imposed on these sections which is comparable to the noise of real samples. Therefore, real samples are evaluated in order to determine how the noise parameters can be defined. Thus, test slices can be evaluated containing a white noise and later be compared with their predefined parameters. Finally, the best results can be tested on a real specimen.

3.1. Determine the noise parameters

To determine the distribution parameters, scans of plane plates are

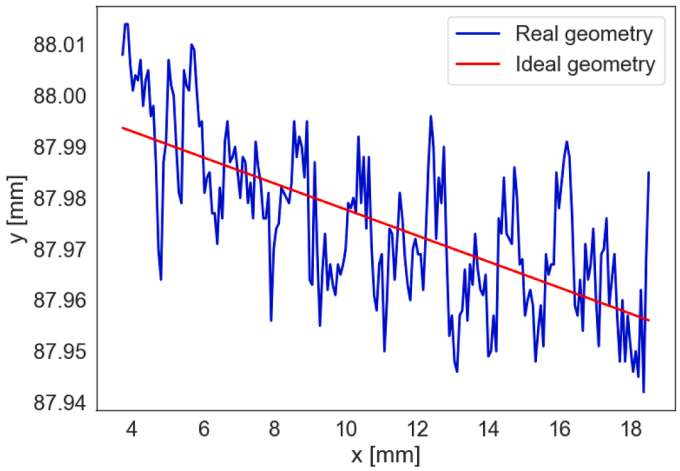

Fig. 4. Even surface with fitted ideal even surface.

evaluated. These are scanned using a 3D laser scanner with a profile resolution of 512 pixels per profile with a scan width of around 36 mm. A total of four specimens is selected. All specimen have the same geometry and rolled surface. Each scanned specimen containing 2700 slices. Every slice consists of 200 data points. A straight line is fitted through these points to represent the ideal geometry (see Fig. 4). The deviation of this straight line is determined at each point to determine the noise. It must be said that the resolution of the laser does not allow the surface roughness to be measured. The noise is therefore more due to the measurement inaccuracy caused by the laser and the movement of the laser.

This method generates over two million data points that can be evaluated. It cannot be ruled out that outliers are present, which are generated by imperfections on the plate surface. The outliers are determined using the Interquartile Range (IQR). The IQR is the difference between the 25th percentile (Q1) and the 75th percentile (Q3). A total of 38,000 outliers are removed. The remaining 2027,540 data points are compared with the following comparison functions:

- Normal distribution
- Lognormal distribution
- Gamma distribution
- Beta distribution
- Alpha distribution

Not all distributions allow negative values, which are necessary for the current evaluation. In this case the distributions will be shifted by using a Location parameter which allows negative values. The density function and the comparison functions can be seen in Fig. 5. To find the closest matching function, the lowest sum square error and Kullback-Leibler divergence (KL-div) is calculated. The results of the evaluation are shown in Table 2.

It turns out that the Gamma distribution is the best fit due to the sum square error and the KL-div being the lowest. The Shape parameter is 2507.51, the Location parameter is −0.59 and the Scale parameter is $2.34{\cdot}10^{-4}$.

3.2. Generation of the test slices

Fillet welds are used as a reference for the test slice description, as the weld toes are much easier to model compared to butt welds. In each slice two weld toes are present which are completely independent from each other. All slices receive a predefined ideal geometry for each weld toe consisting of the weld toe radius and weld toe angle. There is a straight area in front of each weld toe and the area between the weld

Table 2
Comparison of the density function with the comparison functions.

Distribution	Sum square error	KL-div
Gamma	13.7	1.4e-3
Lognorm	14.3	1.4e-3
Norm	18.3	1.5e-3
Beta	59.6	2.6e-3
Alpha	117.2	3.4e-3

Table 3
Mean and mode values of the point distance generated by the laser scanner.

Specimen	Mean-value [mm]	Mode-value [mm]
1	0.074	0.072
2	0.074	0.072
3	0.074	0.072
4	0.076	0.073

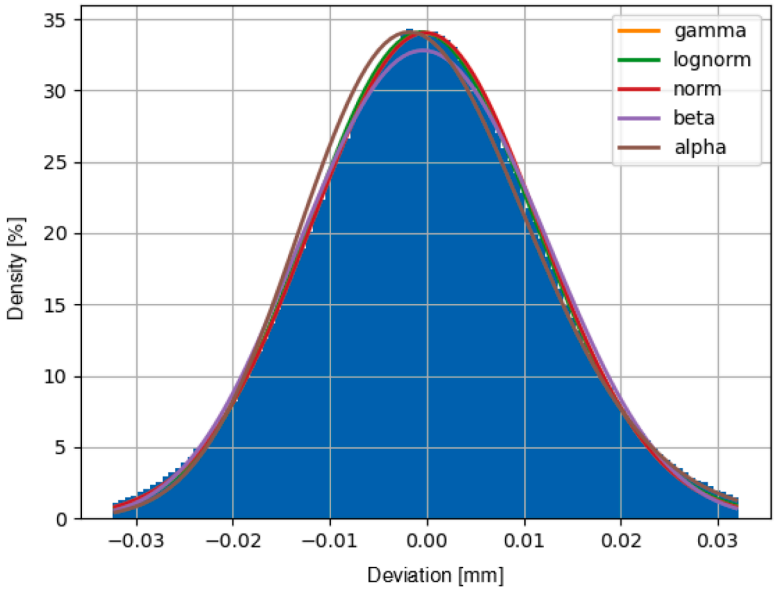

Fig. 5. Density function of the distances to the even range without outliers including comparison functions.

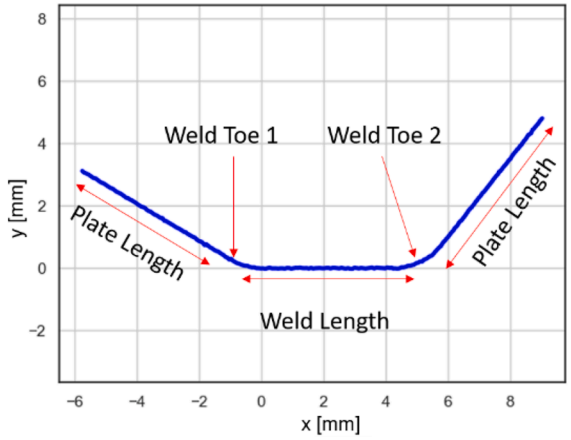

(a) An example of a test slice with the description of the geometry

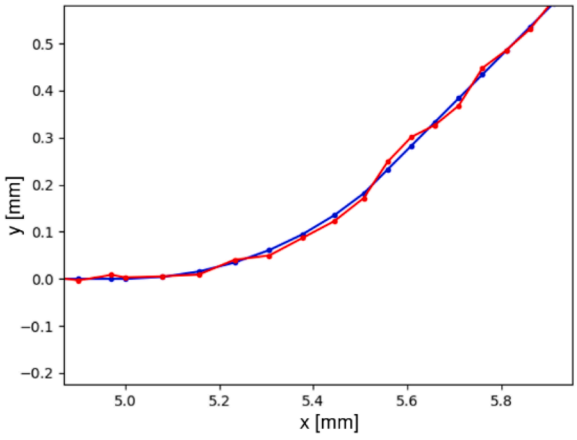

(b) Comparison of the initial geometry (blue) with the noise (red) using an example of a weld toe

Fig. 6. Geometry of the test slices (a) and the effect of the superimposed noise (b).

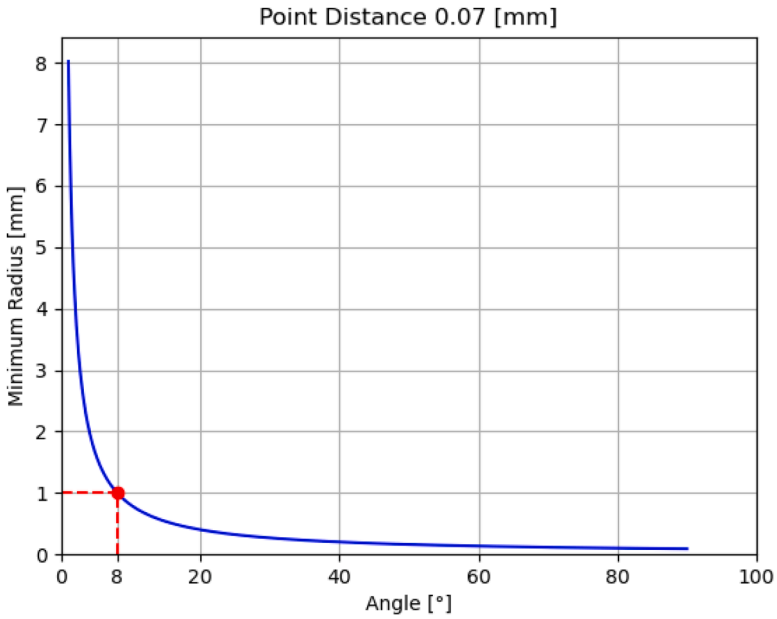

Fig. 7. The minimum radius that can be mapped as a function of the angle and the corresponding angle for a radius of 1 mm is marked.

toes also contains a straight area. Each slice will be represented by a given number of data points. For this purpose, the point distance that is generated by the laser scanner must be determined. The mean and mode values are calculated for the four specimens used to determine the noise. These values are shown in Table 3.

All values are in the range of 0.07. Therefore, this value can be used for all test slices. The noise is superimposed over the test slices with the gamma distribution parameters from Section 3.1. An example of such a test slice can be seen in Fig. 6(a). The effect of the noise on the initial geometry is shown in Fig. 6(b).

This allows randomly distributed weld toe parameters to be generated and applied to the test slices. However, it must be noted that the minimal determinable radius depends on the given point spacing. Each weld toe needs at least three points so that a fixed radius can be applied. In conclusion, the determinable radius depends on the point distance and the weld toe angle α. This fact can be described as,

$$R = \sqrt{\frac{s^2}{\left(1 - \sqrt{1 - \sin\left(\frac{\alpha}{2}\right)^2}\right)^2 + \sin\left(\frac{\alpha}{2}\right)^2}} \tag{3.1}$$

The formula can be converted to α:

$$\alpha = \cos^{-1}\left(\frac{2R^4 - 4R^2s^2 + s^4}{2R^4}\right) \tag{3.2}$$

With the point distance of 0.07 mm the graph shown in Fig. 7 follows. The minimum determinable radius at each angle is shown in Fig. 7.

Every radius and angle combination must therefore lie above this curve. Only then the radius is clearly described. This also avoids errors in the generation of the test slices. The limit values must now be defined for

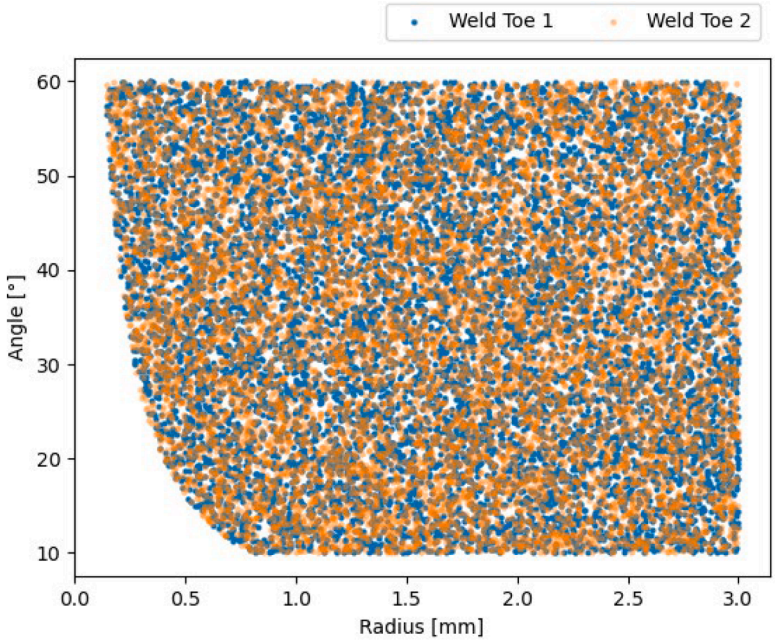

Fig. 8. Parameter distribution of the test slices of both weld toes.

the test slices. This is based on real samples (Schork et al., 2018).

- Radius: 0.1 to 3.0 mm
- Angle: 10 to 60°
- Plate length: 3.0 to 6.0 mm
- Weld length: 2.0 to 8.0 mm

Using these parameter limits and the minimum radius, equally distributed radius and angle combinations can be generated for both weld toes. A total of 10,000 test slices are generated. Thus, two weld toes result in 20,000 combinations. The parameter distribution of the test slices is shown in Fig. 8.

3.3. Initial evaluation of the test slices

Before the filtered sections are evaluated, it is necessary to check how the evaluation of the initial data without the noise proceeds. Thus, the parameter limits or the limits of the cubic parametric spline can be checked on an ideal weld geometry. For this purpose, the 10,000 test slices are used. For the ideal geometry, the only decisive value remains the correction value for the weld toe angle (see Fig. 2). Due to the high impact on the measurement results different correction values needs to be tested. The following correction values are examined:

- 10^{-2}
- 10^{-3}
- 10^{-4}
- 10^{-5}

The differences between the measured value and the initial values are plotted for the different correction values in Fig. 9.

The gray area shows the zone that cannot be evaluated according to the limitation of the minimal determinable radius (see Fig. 7). Smaller correction values produce lower deviations. The results do not show a noticeable difference between 10^{-4} and 10^{-5} for the correction value. Therefore, 10^{-4} can be used for the following evaluations. Note that the correction value was determined using ideal slices without additional noise.

3.4. Finding the best filter parameters

First, all weld toes are to be measured using the best possible parameters. For this purpose, the best parameter pairing is found for each weld toe and each filter function. Since this is a very time-consuming process, an optimization method, that is a Particle Swarm Optimization (PSO), is implemented. The advantage is that the problem to be solved does not have to be differentiable.

The particles P are randomly distributed in the search area and random velocities V are defined. For the next iteration step t, the particle positions X are updated as follows,

$$X^i(t+1) = X^i(t) + V^i(t+1) \tag{3.3}$$

Also, the velocity will be updated by using an inertia w, two cognitive coefficients c and two random numbers r. Therefore, the best particle *pbest* of an iteration and the global best *gbest* is required,

$$V^i(t+1) = wV^i(t) + c_1 r_1 \left(pbest^i - X^i(t)\right) + c_2 r_2 \left(gbest - X^i(t)\right) \tag{3.4}$$

In each iteration step, the best position of the particles is compared with the global best particle. Through several iteration steps, an attempt is then made to approach the best solution. The minimal deviation of radius and angle of a weld toe is evaluated. For this purpose, a percentage deviation is determined for each parameter, which is then summed up. The smallest deviation of the weld toe radius and angle combined will be defined as the best particle.

The necessary parameters of the PSO are used from (Magnus, 2010):

- P: 29
- $r1$: −0.6504
- $r2$: 2.2073
- w: −0.4349

The number of particles is reduced from 29 to 14 in order to speed up the evaluation. With the different number of particles comparable results could be achieved. A v_{max} of 0.1 has been proven to be effective during test runs. The maximum of 400 iteration steps from (Magnus, 2010) is used as termination criterion. However, this value is not reached in any of the cases. The second termination criterion is decisive. Here, the iteration is terminated as soon as the same percentage

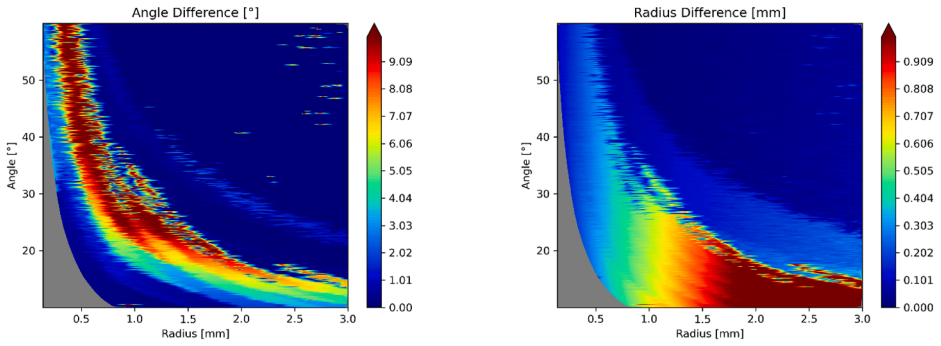

(a) Correction-value 10^{-2}

(b) Correction-value 10^{-2}

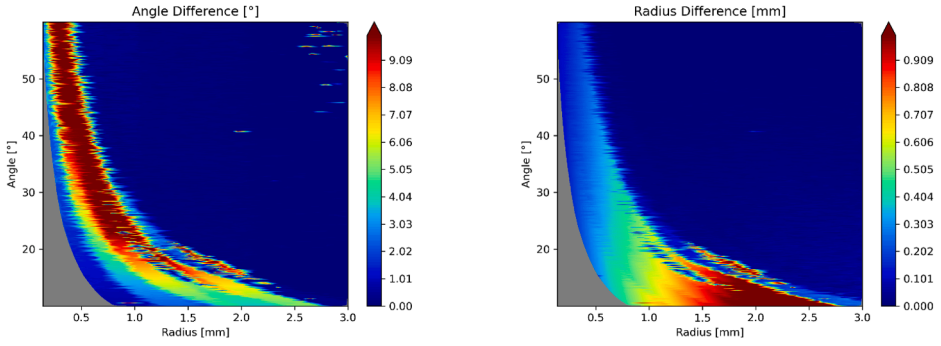

(c) Correction-value 10^{-3}

(d) Correction-value 10^{-3}

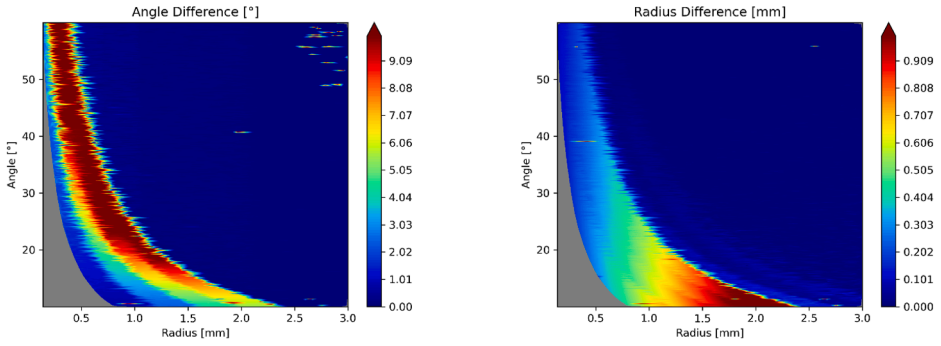

(e) Correction-value 10^{-4}

(f) Correction-value 10^{-4}

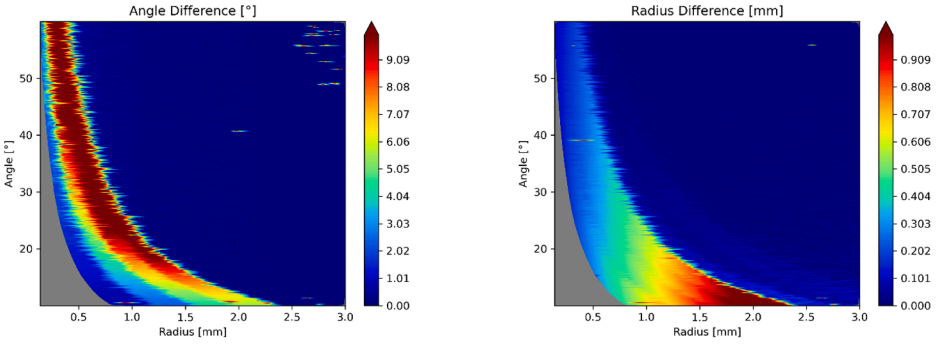

(g) Correction-value 10^{-5}

(h) Correction-value 10^{-5}

Fig. 9. Deviations of the angle and the radius from the initial values for the different correction values.

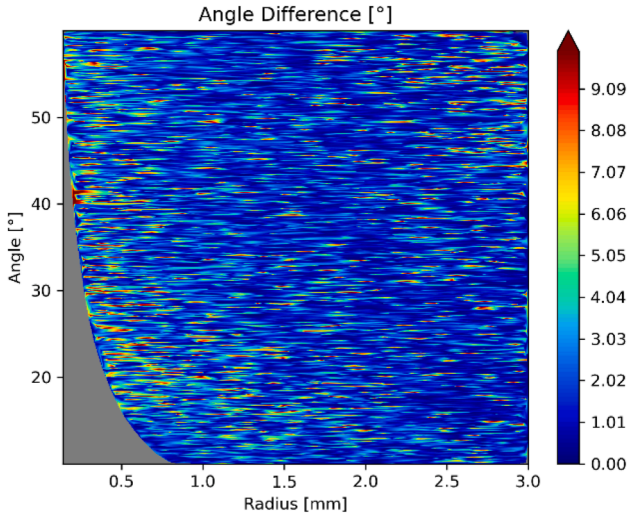

(a) Angle deviation with the global method

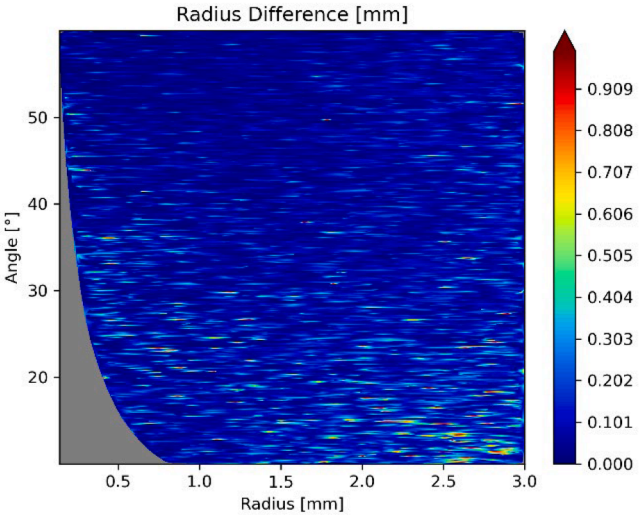

(b) Radius deviation with the global method

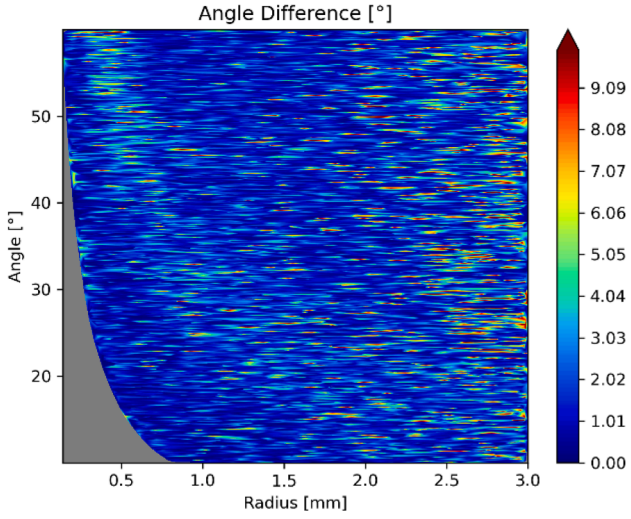

(c) Angle deviation with the local method

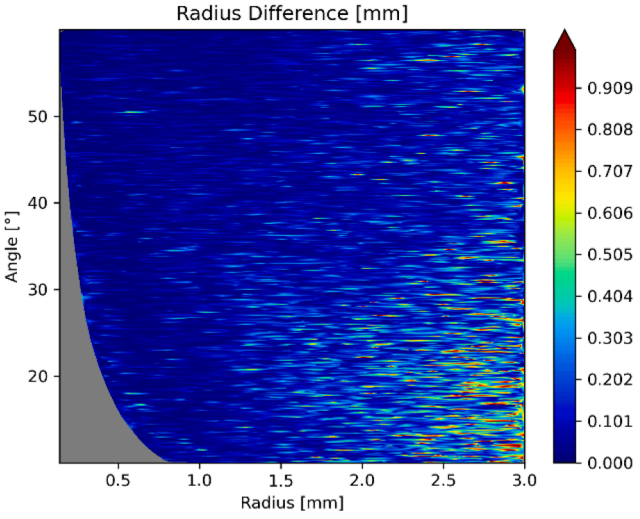

(d) Radius deviation with the local method

Fig. 10. Deviations of the weld toe parameters for the B-Spline filter function.

deviation occurs four times in a row as the best choice. This prevents too many iterations, since it has been shown that in the rarest cases a better result could be found afterwards.

For the slice evaluation, a distinction is made between the local and the global method (see Fig. 3). In the local method, the search radius is of great importance, since it has a significant influence on the local smoothing due to the extension of the filtered area. With the global filter areas, the search radius is only used to find the weld toes. Here, it is advisable to select the search radius as large as possible, so that the weld toes found are more reliable. By fixing this parameter to 4 mm, iteration steps can be reduced. In all cases, both the x and the y values are filtered separately. Exceptions are the Polynomial and the B-spline filter functions. The parameter limits are determined for each filter by test runs.

3.4.1. B-Spline filer

The B-Spline could be used for both filter areas without difficulty and the results can be seen in Fig. 10.

The B-spline shows very small deviations from the initial values in both cases. Excellent results are obtained in all areas. The errors are mostly limited to single parameter pairings. Overall, the filter is apt to map a weld toe.

3.4.2. Gaussian filter

Both filter areas could be used for the Gaussian filter. The results are shown in Fig. 11.

Except for some outliers in the boundary area of the angular deviation, the results are satisfyingly good. In addition, it must be emphasized that both local and global methods provide similarly good results. Thus, this filter is apt.

3.4.3. Lowess filter

The Lowess filter could be used for both methods without difficulty.

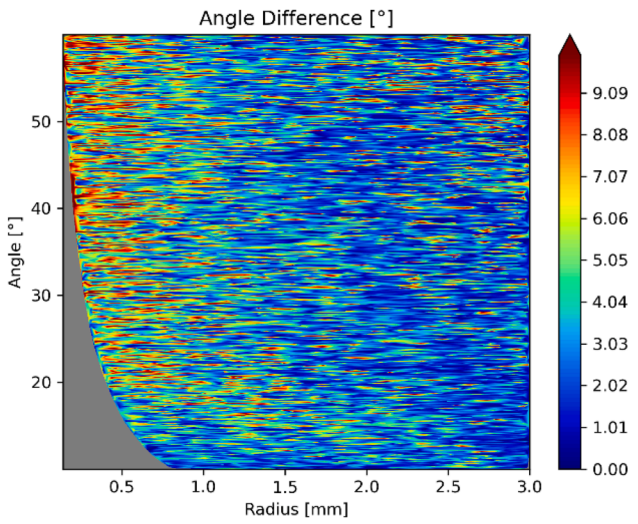

(a) Angle deviation with the global method

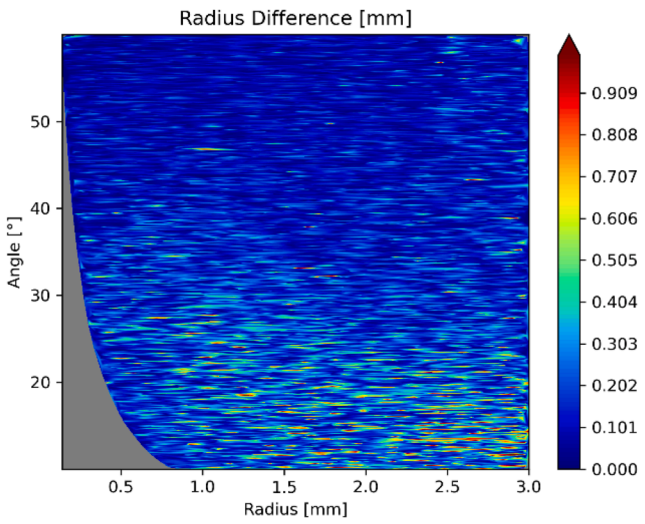

(b) Radius deviation with the global method

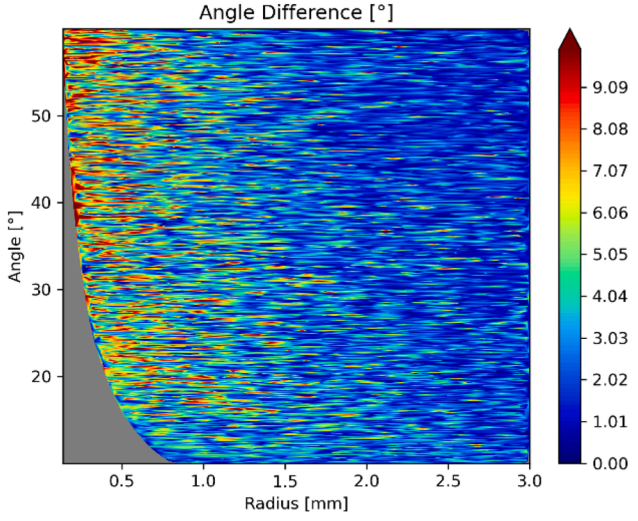

(c) Angle deviation with the local method

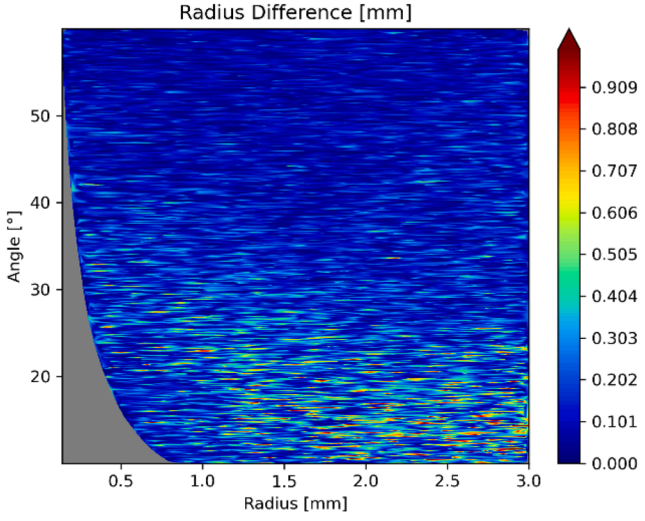

(d) Radius deviation with the local method

Fig. 11. Deviations of the weld toe parameters for the Gaussian filter function.

The deviations are shown in Fig. 12.

The angular deviations are sometimes considerable, especially in the boundary areas. The radius, on the other hand, is quite well resolved in the local method. With the global method, the representation is quite good in the boundary area. In the remaining area there are larger deviations.

3.4.4. Lowpass filter

The Lowpass filter is only suitable for the global evaluation. For the local evaluation, the areas are often too small and the weld toe cannot be mapped. The results for the global filter area are shown in Fig. 13.

With the exception of a few outliers, the global evaluation has a considerably high mapping accuracy in all areas.

3.4.5. Moving average filter

For the Moving Average filter function, the evaluation with the local method is aborted due to a high error rate of the results. It is not possible to achieve valid results with this filter area. An evaluation of the global method is possible and the results can be seen in Fig. 14.

The radius shows unsatisfactory results especially with large radii and small angles. This range is quite pronounced and erroneous measurements occur. The angle determination is quite inaccurate for all ranges. This filter is therefore inapt.

3.4.6. Polynomial filter

The Polynomial filter is easily applicable for both methods. In Fig. 15 the results of the deviations can be seen.

The local method shows only small deviations while the global method shows a high deviation of the radius in the boundary area. However, the angular deviation is small for both cases. All in all, the filter function is apt to map weld toes.

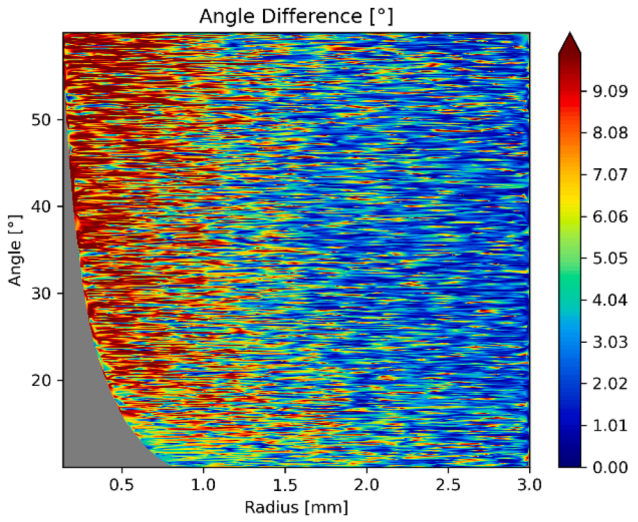

(a) Angle deviation with the global method

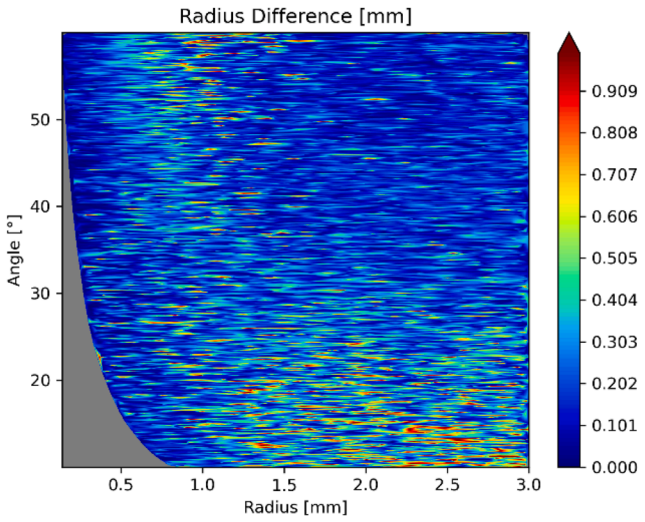

(b) Radius deviation with the global method

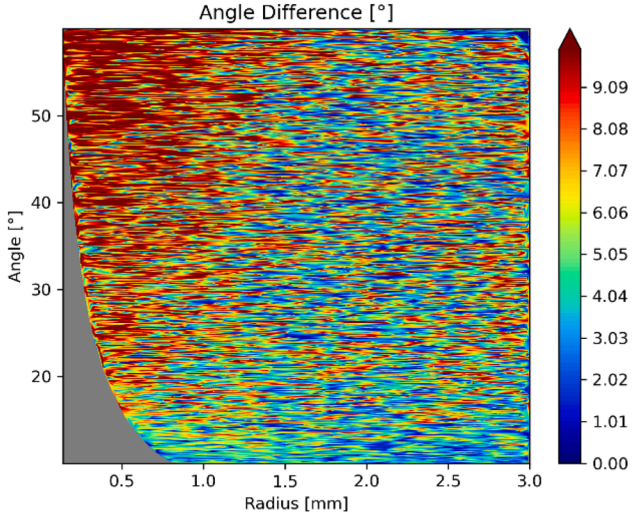

(c) Angle deviation with the local method

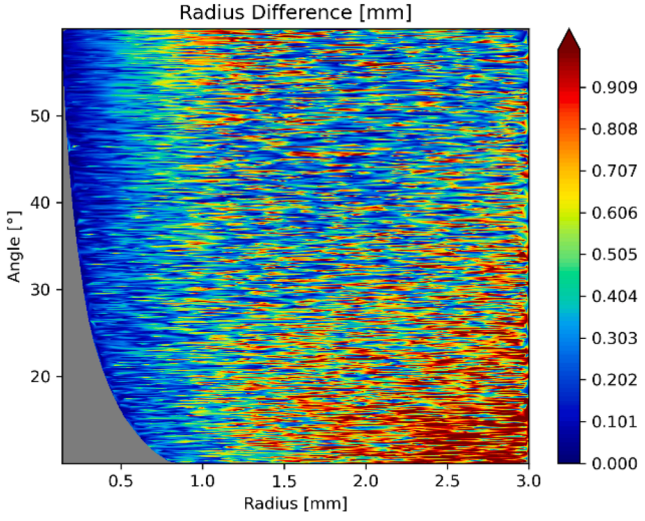

(d) Radius deviation with the local method

Fig. 12. Deviations of the weld toe parameters for the Lowess filter function.

3.4.7. Savitzky-Golay filter

The Savitzky-Golay filter is applicable for both methods without difficulty. The results are shown in Fig. 16.

Except for isolated outliers in the boundary area and the depiction of large radii at small angles, the Savitzky-Golay filter achieves good results in both local and global evaluation.

3.4.8. Summary

With the PSO each of the 20,000 combinations of radii and angles are tested with specific input parameters for the filter functions. For instance, for the B-Spline filter function 1230 unique parameters (global filtering method) are required for the evaluation of the radii and angles, for the Lowess filter function, however, only 11 are required (see Table 1).

As the same input parameters occur for some combinations, the unique parameters are counted for each filter function and method (see Table 1). Since a universally applicable filter can be defined as needing a low number of parameters, the quality of the methods can be examined by assessing the number of unique parameters needed. This number of unique parameters is shown in Table 4 for each filter function and filter area.

The B-Spline filter shows only minor divergences for both filter areas which can be seen in Fig. 10. However, it is shown in Table 4 that the filter needs a large number of unique parameters especially for the local filter area. Although it produces good results, it requires a finely adjusted set of parameters which can be led back to its three input parameters. Therefore, the approximate weld toe geometry would have to be known in order to produce valid results with such a sensitive filter function. However, since the weld toe geometry is usually not known in reality, the B-Spline filter is not universally applicable.

For the Gaussian filter, good results with a small number of unique parameters could be achieved for the global and local filter area (see

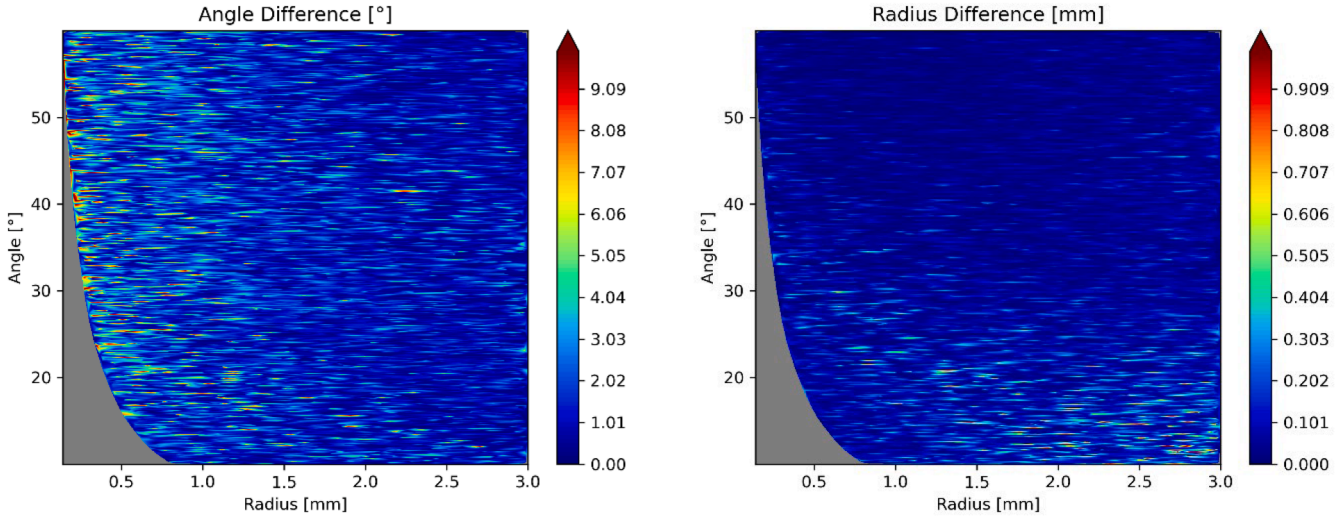

(a) Angle deviation with the global method

(b) Radius deviation with the global method

Fig. 13. Deviations of the weld toe parameters for the Lowpass filter function.

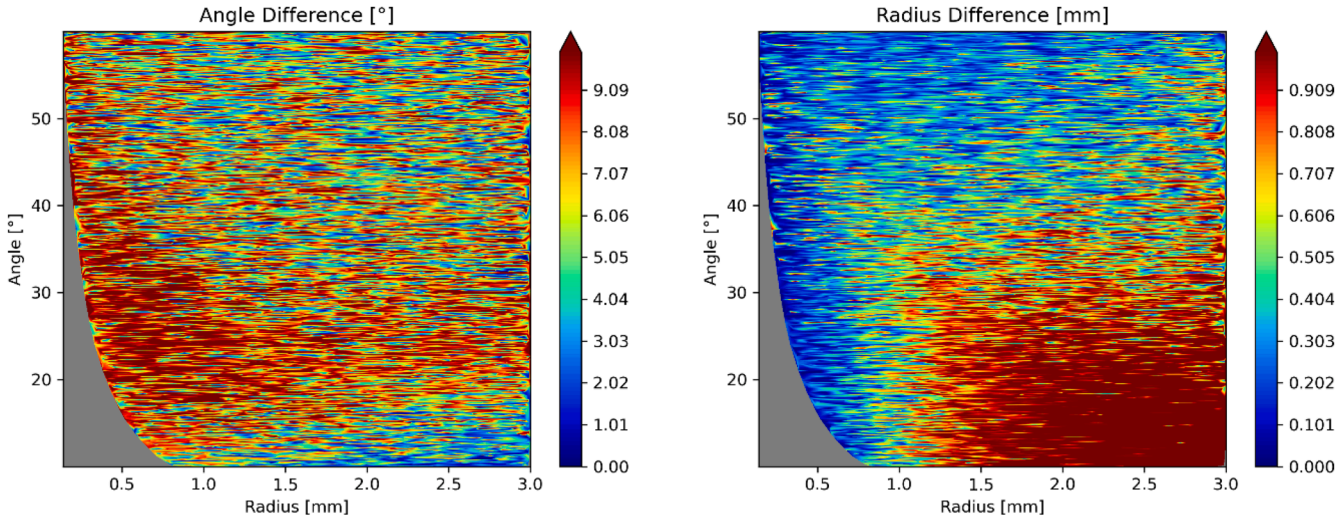

(a) Angle deviation with the global method

(b) Radius deviation with the global method

Fig. 14. Deviations of the weld toe parameters for the Moving Average filter function.

Fig. 11). These are solid requirements for a universally applicable filter function and applies to both filter areas.

The Lowess filter function does not require many unique parameters. However, it is not suitable as a universal filter due to the high angular divergence for both filter areas which can be seen in Fig. 12.

Although the Lowpass filter function requires a larger amount of unique input parameters, it produces satisfactory results (see Fig. 13). Therefore, it can be used as a universal filter function as a global filter area.

The Moving Average filter requires the least amount of unique input parameter. However, the divergence for both filter areas, which can be seen in Fig. 14, shows that the filter function is not able to describe the weld toe geometry sufficiently. Therefore, the filter function is inapt as a universal filter.

Especially the local filter area for the Polynomial filter function shows only small divergences (Fig. 15). Also, the small number of unique input parameters for both filter areas (Table 4) meets the requirements of a universal filter.

The Savitzky-Golay filter function shows only small divergences for the radius and angle for both filter areas (see Fig. 16). Due to the fact that the number of unique input parameters is also small, the filter function is apt as a universal filter.

3.5. Examination of the universal filters

As mentioned above, few filter functions have the potential to be an apt universal filter since they produce good results using relatively few unique parameters: The Gaussian filter, Lowpass filter, Polynomial filter

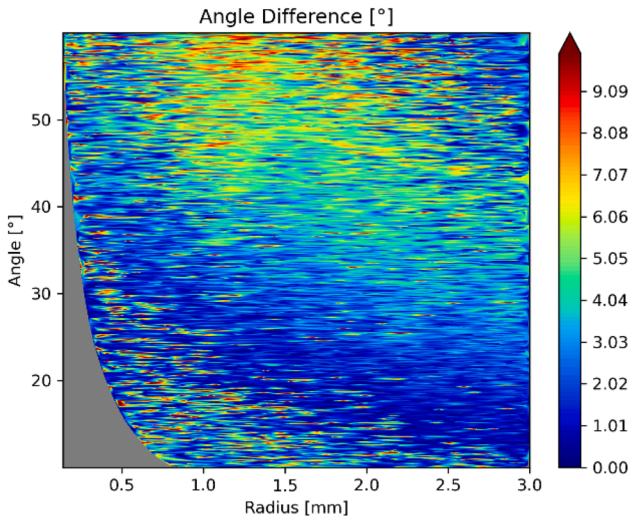

(a) Angle deviation with the global method

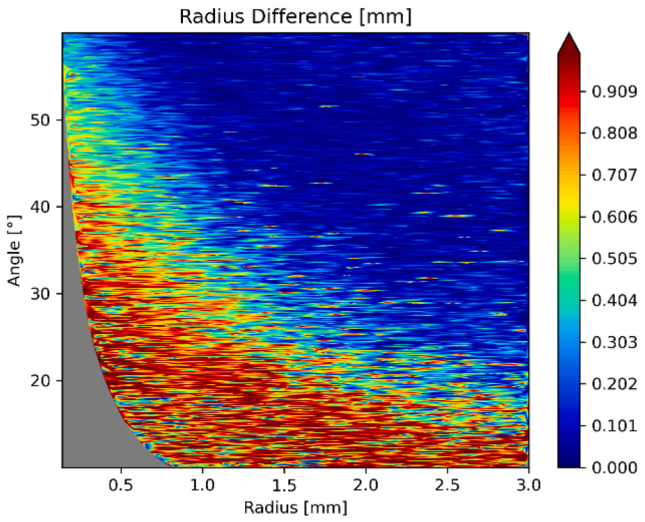

(b) Radius deviation with the global method

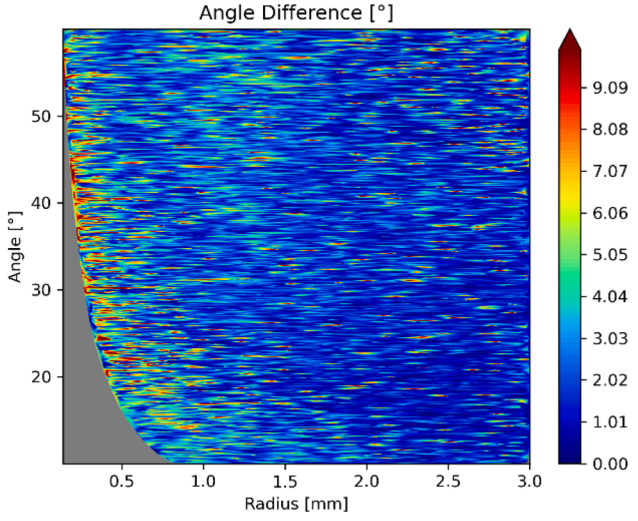

(c) Angle deviation with the local method

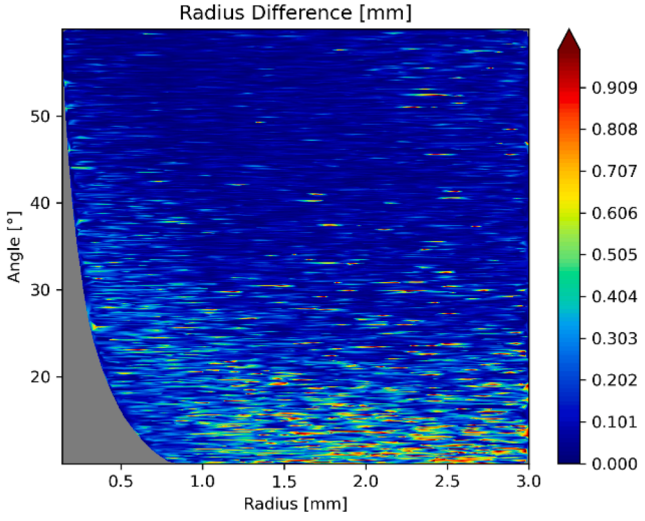

(d) Radius deviation with the local method

Fig. 15. Deviations of the weld toe parameters for Polynomial filter function.

and Savitzky-Golay filter. Except for the Lowpass filter, both filter areas are used.

To determine the most suitable filter function, a statistical evaluation of the best parameters from Section 3.4 will be conducted. Therefore, the mean, median and mode values of the parameters will be compared for each filter function and method. Additionally, the four most common parameters, referred to as Mode1 to Mode4, will be examined to ensure a diverse range of input parameters. The subsequent evaluation of the test slices will be based on these fixed parameters for each statistical value.

To determine the optimal filter parameters for each function and method, the Root-Mean-Square-Error (RMSE) and the Mean-Absolute-Error (MAE) will be used. Since both methods can be influenced by outliers, the deviations are filtered by using the IQR Method beforehand, since strong deviations indicate measurement errors, which can certainly occur. To ensure that no inaccurate measurements are classified as outliers, the interquartile range from 10% to 90% is evaluated. The RMSE and MAE values are calculated for the radius and the angle. Both values can be combined by using the mean value. With this procedure, the parameter combination with the lowest error can be selected for each filter function and filter area. The best filter results are shown in Table 5.

The results in Table 5 show a better performance of the global filter area in comparison to the local method. Since the local method with the search radius has always one more parameter that influences the results, the global method is more useable. For this reason, only the global Gaussian, Lowpass and Polynomial filter functions will be used for further investigations because of the lower error.

To improve the performance of the chosen filter functions, the correction value for the angle calculation will be adjusted again. The small value of 10^{-4} of the initial evaluation (see Section 3.3) is inapt for the filtered data since it was calculated using artificial slices, i.e. without the presence of noise. Due to the noise of the test slices, strong local slope

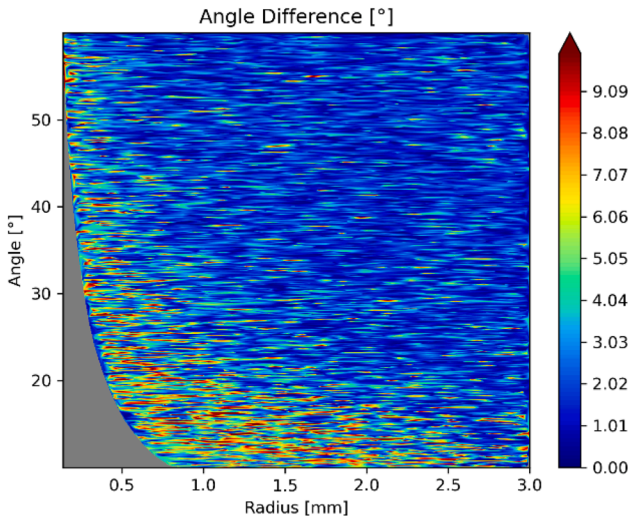

(a) Angle deviation with the global method

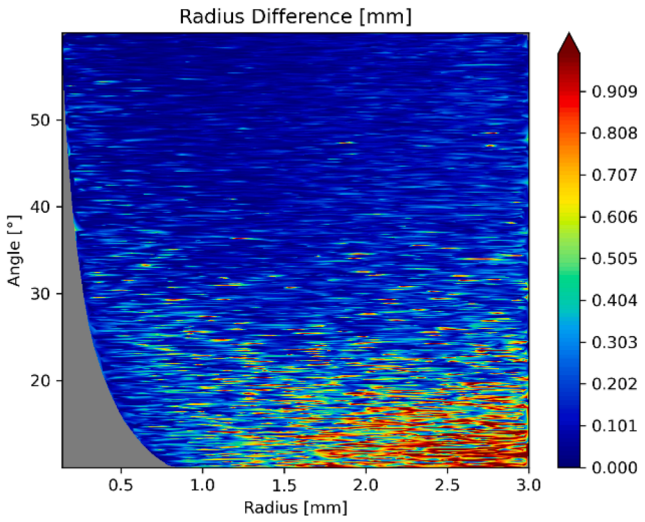

(b) Radius deviation with the global method

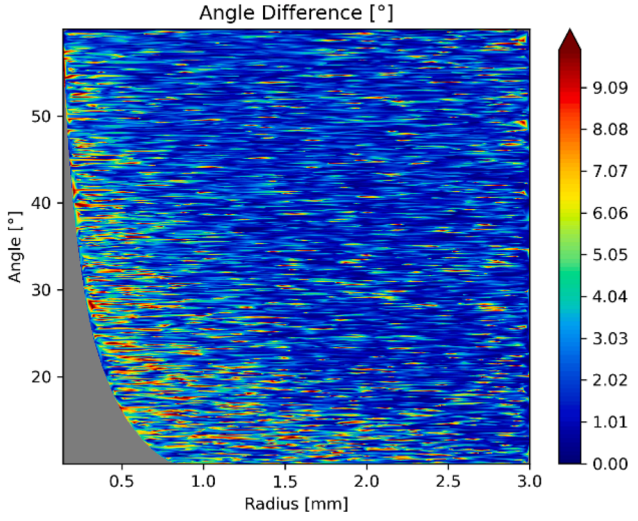

(c) Angle deviation with the local method

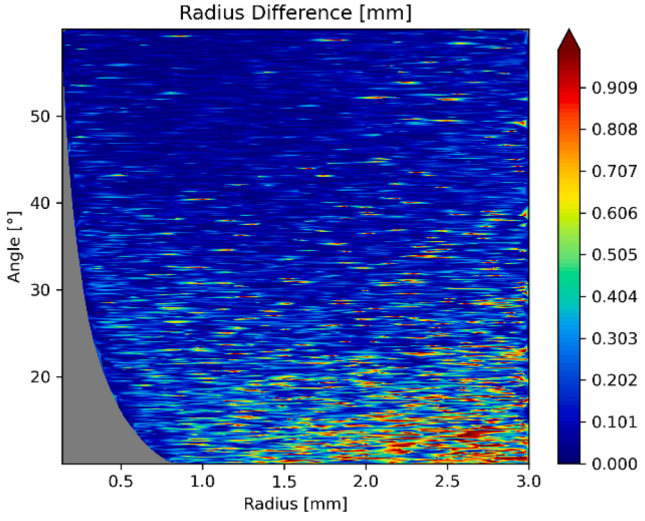

(d) Radius deviation with the local method

Fig. 16. Deviations of the weld toe parameters for Savitzky-Golay filter function.

Table 4
Unique parameters per filter function and filter area.

Filter functions	Local filter method	Global filter method
B-Spline	13,330	1230
Gaussian	143	31
Lowess	168	11
Lowpass	–	432
Moving Average	–	8
Polynomial	232	38
Savitzky-Golay	1570	316

changes can occur, especially at the weld toes. Thus, the correction value has to be increased to 10^{-2}. This enables angular measurements close to the plane areas at the weld toe boundary due to all chosen filter functions being able to smooth these areas satisfactorily. The impact on the RMSE and MAE values of the lower correction is shown in Table 6.

The following parameters for the different filter functions will be used:

- Gaussian filter function:
  - Standard deviation: 2
- Lowpass filter function:
  - Cut-off frequency: 0.16
  - Degree of the filter: 6
- Polynomial filter function:
  - Polynomial degree: 30

In all cases, the global filter area is used with a search radius of 4 mm.

For a better comparison, a contour plot of the deviations with a grid is done (see Fig. 17).

The Gaussian, Lowpass and Polynomial filter functions have a lower

Table 5
Best fit parameters for each filter function and filter area with the error measures.

Filter function	Filter area	Best parameters	Error measures					
			Radius		Angle		Combined	
			RMSE	MAE	RMSE	MAE	RMSE	MAE
Gaussian	Local	Average	0.542	0.382	8.639	5.810	4.591	3.100
	Global	Average	0.481	0.346	6.650	4.645	3.566	2.495
Lowpass	Local	–	–	–	–	–	–	–
	Global	Mode4	0.454	0.311	6.413	4.150	3.433	2.231
Polynomial	Local	Mode1	1.109	0.782	15.806	10.676	8.457	5.729
	Global	Mode	1.042	0.667	9.915	6.133	5.479	3.400
Savitzky-Golay	Local	Mode	0.901	0.629	13.958	9.119	7.429	4.874
	Global	Mode1	0.909	0.667	13.048	8.482	6.978	4.575

Table 6
Influence of the correction value of the different filter functions with the global method.

Filter Function	Correction Value	Error measures					
		Radius		Angle		Combined	
		RMSE	MAE	RMSE	MAE	RMSE	MAE
Gaussian	10^{-4}	0.481	0.346	6.650	4.645	3.566	2.495
	10^{-2}	0.421	0.277	4.090	2.938	2.256	1.608
Lowpass	10^{-4}	0.454	0.311	6.413	4.150	3.433	2.231
	10^{-2}	0.368	0.254	2.364	1.870	1.365	1.062
Polynomial	10^{-4}	1.042	0.667	9.915	6.133	5.479	3.400
	10^{-2}	0.828	0.532	3.722	2.712	2.275	1.622

error for the radius and the angle using the adjusted correction value of 10^{-2}. In Fig. 17(f), it can be seen that the boundary area of the radius of the Polynomial filter has a relatively high divergence in comparison to the Gaussian and Lowpass filter function. The other two filters produce significantly better results and the Polynomial filter has no advantages in comparison. Overall, the Lowpass filter shows the best results but the radius deviation of the Gaussian Filter is better in the boundary area. For this reason, both filters will be used for further applications. Due to the fact that the Lowpass filter and Gaussian filter achieve good results with only one parameter pairing, these two filters are well suited as universal filters.

3.6. Testing of a reference specimen

To verify the results, the filters are to be tested on a real specimen scanned using the same laser scanner which is used for the previous procedure. A reference specimen made by wire-cut electrical discharge machining (EDM) within the Round Robin study of the International Institute of Welding (IIW) on weld geometry measurements is used for this purpose (Jung et al., 2024). The specimen has a total of four fillet welds and thus eight weld toes with specified parameters. The weld toes are labeled A to H and the related weld toe parameters are shown in Table 7.

The 10 mm wide seams are subdivided into 100 slices for evaluation. All slices will be evaluated using the Gaussian and Lowpass filter function with the parameters from Section 3.5. For the parameters, the mean, median and, if available, the mode values are considered. Due to the small sample of 100 slices, a uniform mode value cannot be found for each weld toe by using three digits. The results of the weld toe radius are shown in Table 8 and of the weld toe angle in Table 9.

It can be seen that often no mode evaluation is possible for the angle, since multiple values do not always occur within 100 slices. Boxplots are used for a better depiction of the data. These can be seen in Fig. 18. For the evaluation of the deviations a tolerance range is introduced by using the minimum measurable values. If Formula 3.1 is used, a minimum measurable radius of 0.179 mm would be possible using a point spacing of 0.07. For that reason, a deviation of 0.2 mm is tolerated for the radius. In Table 7 it can be seen that the radius of weld toe F is below the minimal radius, which explains the high deviation (see Table 8). With Formula 3.2 the minimum measurable angle can also be calculated. Since there are several radii, a single tolerance value is not possible (see Table 10). Therefore, a conservative approach is used taking the smallest measurable angle of 1.5°, which is defined by the largest radius of 5.3 mm.

The tolerance range (green) is shown in the plot (see Fig. 18). Only the absolute deviations of the machined value are shown since they describe real applications more efficiently than the relative deviations. In the box plots, the median is shown in the IQR-box. The lower part of the IQR-box represents the 25th percentile (Q1) and the upper part represents the 75th percentile (Q3). For the lower whisker Q1–1.5·IQR defines the minimum and for the upper whisker Q3+1.5·IQR defines the maximum.

The Gaussian filter function has an acceptable accuracy for the radius. However, the angular deviation is higher compared to the Lowpass filter. Since the radius deviation is also smaller, the Lowpass filter is considered superior in terms of accuracy compared to the Gaussian filter function. Nearly all interquartile ranges fall within the tolerance range for radius deviation. The angular measurement has a higher deviation and exceeds the tolerance area. However, except for weld toe B, all median values fall within the tolerance range (see Table 9). The radius deviation of the weld toe F is noticeable. The deviation is clearly higher compared to the other weld toes. It must be said that the manufactured weld toe has no clear radius definition. It was produced as a sharp edge with a wire radius of 0.15 mm. Such a small radius cannot be mapped accurately due to the point distance only allowing a minimal radius of 0.179 mm. Unfortunately, the threshold of the tolerance values is not met by all weld toes. The Lowpass filter function achieves measurement results within the tolerance range for radii which are above the minimal possible radius. For the angular measurement a higher deviation occurs which exceeds the defined tolerance range. It must be noted that a conservative approach was used to determine the tolerance range, i.e. the largest radius was used. Since the tolerance range depends on the radius, it would be larger if another radius are to be used for the definition (see Table 10).

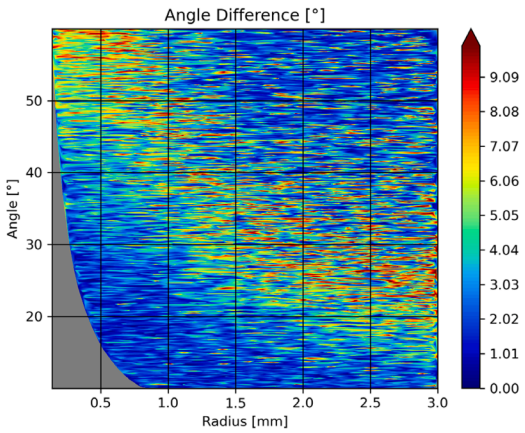

(a) Gaussian angle deviation (RMSE: 4.090, MAE: 2.938)

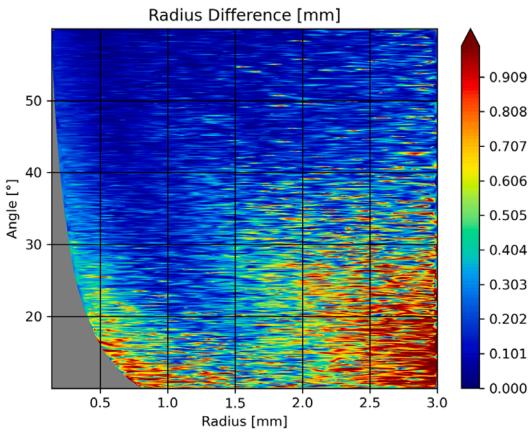

(b) Gaussian radius deviation (RMSE: 0.421, MAE: 0.277)

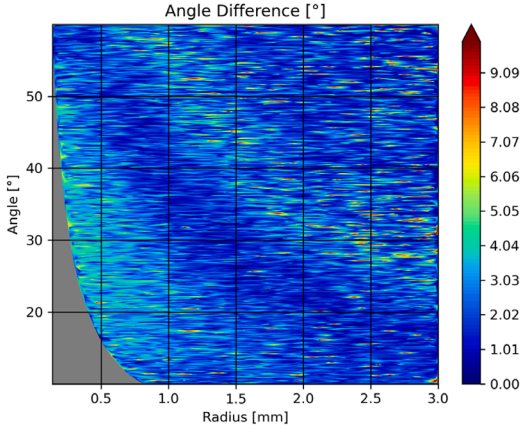

(c) Lowpass angle deviation (RMSE: 2.364, MAE: 1.870)

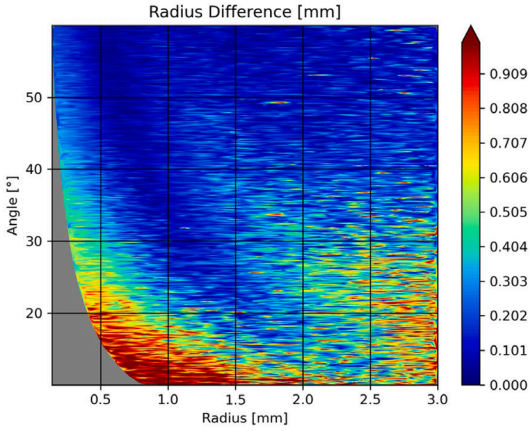

(d) Lowpass radius deviation (RMSE: 0.368, MAE: 0.254)

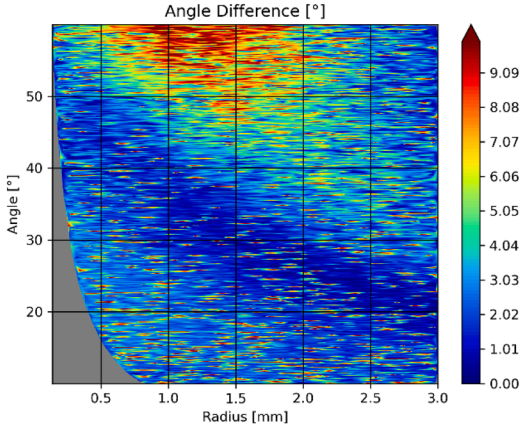

(e) Polynomial angle deviation (RMSE: 3.722, MAE: 2.712)

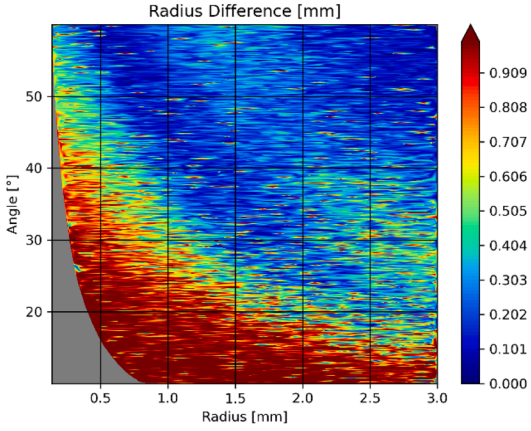

(f) Polynomial radius deviation (RMSE: 0.828, MAE: 0.532)

Fig. 17. Deviations of the different filter functions measured with the most suitable input parameters and a correction value of 10^{-2}.

Table 7
Weld Toe Parameters of the reference specimen.

Weld toe	Weld toe radius [mm]	Weld toe angle [°]
A	3.1	45
B	1.2	45
C	4.1	45
D	5.3	45
E	1.5	45
F	0.15	45
G	0.5	45
H	1.9	45

4. Discussion

A universally applicable filter should allow for precise contour smoothing while operating with fixed input parameters. Almost all of the examined filter functions effectively eliminated noise. However, the Lowess and Moving Average filters proved unsuitable, as they were unable to successfully smooth the 2D sections. Despite its strong performance, the B-Spline filter is not suitable for universal use due to its reliance on highly specific input parameters.

The best results were obtained using the Gaussian and Lowpass filters, which aligns with previous findings where Gaussian filters have been successfully applied to similar tasks (Rohani Raftar et al., 2024). Both the Savitzky-Golay and Polynomial filters were discarded, as they showed larger deviations compared to the other filters. In practical tests on a real specimen, the Lowpass filter performed slightly better than the

Table 8
Mean, median and mode value of the radius compared to the machined weld toe radius of each filter function in mm.

		Gaussian			Lowpass		
Weld toe	Machined [mm]	Mean [mm]	Median [mm]	Mode [mm]	Mean [mm]	Median [mm]	Mode [mm]
A	3.1	2.965	3.050	2.936	2.945	2.945	2.945
B	1.2	1.288	1.297	1.279	1.212	1.211	1.205
C	4.1	4.291	4.243	4.187	4.18	4.156	4.076
D	5.3	5.293	5.348	5.416	5.229	5.229	5.229
E	1.5	1.402	1.486	1.358	1.484	1.507	1.523
F	0.15	0.565	0.566	0.592	0.619	0.6225	0.569
G	0.5	0.665	0.652	0.614	0.718	0.722	0.779
H	1.9	1.934	1.934	2.087	1.861	1.866	1.845

Table 9
Mean, median and mode value of the angle compared to the machined weld toe angle of each filter function in °.

		Gaussian			Lowpass		
Weld toe	Machined [°]	Mean [°]	Median [°]	Mode [°]	Mean [°]	Median [°]	Mode [°]
A	45	41.049	43.14	43.14	43.074	43.660	43.664
B	45	42.351	42.767	–	44.014	48.893	44.388
C	45	43.639	43.901	–	43.719	44.186	45.248
D	45	42.212	43.981	–	42.397	43.564	–
E	45	39.576	42.431	35.736	45.112	45.914	47.853
F	45	39.356	39.1545	38.194	45.439	45.493	45.493
G	45	37.209	36.964	37.554	45.352	43.478	44.793
H	45	43.105	43.976	41.174	44.888	45.340	–

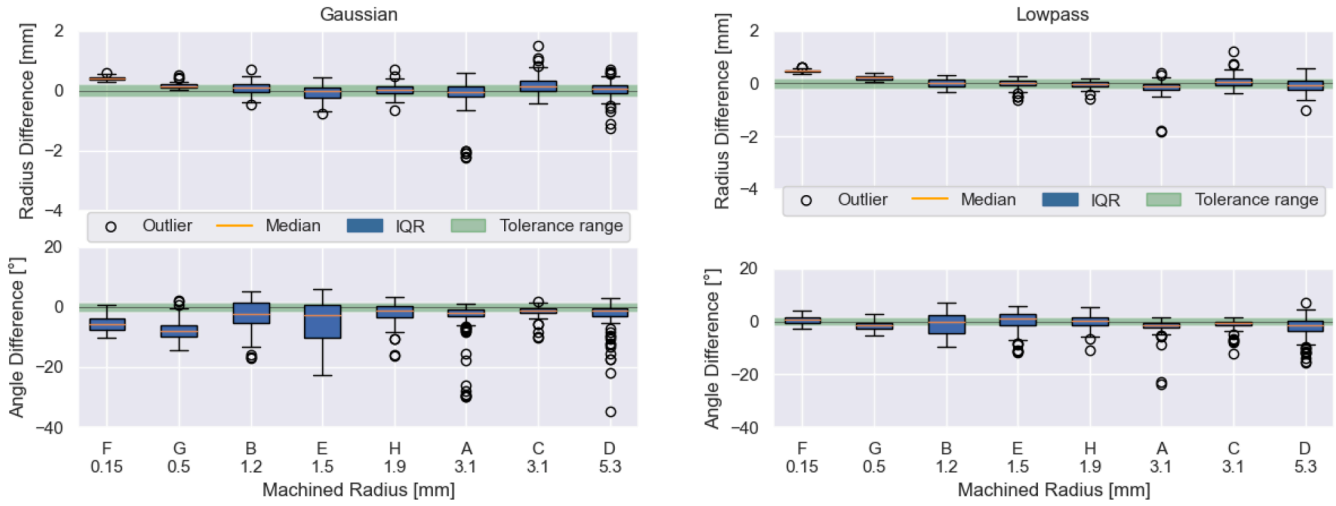

(a) Divergence Gaussian *(b) Divergence Lowpass*

Fig. 18. Absolute divergence of the radius and the angle as boxplot sorted by the machined radius.

Table 10
Minimum measurable angle for the different weld toes with a point distance of 0.07 mm by using Formula 3.2.

Weld Toe	Radius [mm]	Minimum Measurable Angle [°]
A	3.1	2.588
B	1.2	6.685
C	4.1	1.956
D	5.3	1.514
E	1.5	5.348
F	0.15	53.974
G	0.5	16.056
H	1.9	4.222

Gaussian filter, making these two the most favorable filtering methods.

The calibration results presented are device-dependent. When using a different scanner, the calibration must be repeated. The noise of the measured values depends on the laser scanner used and must be determined beforehand, as described in Section 3.1. It is important to note that adjustments to the measurement setup or the laser scanner itself can also affect the noise levels, potentially requiring a new calibration even if the scanner remains unchanged. The calibration method can be extended to other scanners as long as they produce consistent noise patterns. Future work should aim to test the calibration method with different scanners to validate its robustness and adaptability to varying noise characteristics.

Additionally, studies such as Schubnell et al. (2020), Jung et al. (2024), Renken et al. (2024) have already compared various measurement systems, albeit with different measurement methods. These works demonstrate the diversity of measurement systems currently in use. Building on these studies could further strengthen the understanding of how different scanning systems might influence calibration results and filter applicability.

5. Conclusion

Laser-scanned weld seams are more and more used to determine the fatigue strength by using the local weld toe parameters. The advantage of such scans is that a mathematical description of the seam geometry can be made, allowing reproducible measurement results. In this study a calibration method for a laser-scanner-based weld toe measurement was presented. The characteristic of the laser scanner was evaluated and representative test slices were produced and were tested using different filter areas and filter functions. The best results were determined using a PSO. With a comparison of the achieved divergences of the weld toe measurements, the best filter version could be determined. The following observations and conclusions are made:

- The noise characteristic of a laser scanner can be determined by evaluating a measurement of an even surface and determine the most fitting distribution function. In this case the Gamma distribution was best fitting.
- For a calibration of the laser scanner, generated test slices with predefined weld toe geometry can be utilized in large numbers for calibration. The noise characteristic of the laser scanner needs to be applied to the test slices.
- The resolution of the weld toe radius is restricted by the point distance of the measured weld slices.
- Global filtering of a whole slice is superior compared to the local smoothing of the weld toes. The results are more accurate and the global method does not need a parameter which defines the size of the filter area like the local method.
- Some filter functions are not suitable for measuring weld toes. A Moving Average and a Lowess filter cannot map a weld toe sufficiently. A B-Spline can produce a close approximation of the weld toe geometry but only with a fine adjustment of the input parameters. That requires the knowledge of the weld toe geometry which makes this filter function inapt.
- The filtering of the weld toes by using a Gaussian, Lowpass, Polynomial or Savitzky-Golay filter function can produce valid results. Especially the Lowpass and the Gaussian filter perform sufficiently because they are well suited to filter out certain frequencies due to their mathematical description.
- The accuracy of the measurements can be measured by using a tolerance range which is defined by the theoretically smallest radius and angle.
- A universal filter for a wide range of different weld toes is possible. With the combination of a laser scanner and a calibrated universal filter, the measurement of different weld toes with a high measurement accuracy of the weld toe radius is possible.

By applying the developed method, it was possible to calibrate a Lowpass filter for a specific laser scanner. This allows the measurement of a wide range of weld toe geometries by using just one parameter set for the filter function. The measured values for the weld toe radius were predominantly within the tolerance range, while those for the weld toe angle frequently exceeded the tolerance range. However, the definition of such a tolerance range requires further research as it depends on the initial geometry parameters and would therefore not be fixed along a weld seam.

Declaration of generative AI and AI-assisted technologies in the writing process

During the preparation of this work the authors used ChatGPT in order to check spelling and grammar. After using this tool, the authors reviewed and edited the content as needed and take full responsibility for the content of the publication.

CRediT authorship contribution statement

Finn Renken: Writing – review & editing, Writing – original draft, Visualization, Validation, Software, Resources, Project administration, Methodology, Investigation, Formal analysis, Data curation, Conceptualization. **Matthias Jung:** Writing – review & editing. **Sören Ehlers:** Writing – review & editing, Supervision, Resources. **Moritz Braun:** Writing – review & editing, Supervision, Resources.

Declaration of competing interest

The authors declare that they have no known competing financial interests or personal relationships that could have appeared to influence the work reported in this paper.

Data availability

Data will be made available on request.

References

Alam, M.M., Barsoum, Z., Jonsén, P., Kaplan, A., Häggblad, H., 2010. The influence of surface geometry and topography on the fatigue cracking behaviour of laser hybrid welded eccentric fillet joints. Appl. Surf. Sci. 256 (6), 1936–1945. https://doi.org/10.1016/j.apsusc.2009.10.041.

Amir, Y.M., Thörnberg, B., 2017. High precision laser scanning of metallic surfaces. Int. J. Opt. 2017, 1–13. https://doi.org/10.1155/2017/4134205.

Braun, M., Kellner, L., 2022. Comparison of machine learning and stress concentration factors-based fatigue failure prediction in small-scale butt-welded joints. Fatigue Fract. Eng. Mater. Struct. 45 (11), 3403–3417. https://doi.org/10.1111/ffe.13800.

Braun, M., Neuhäusler, J., Denk, M., Renken, F., Kellner, L., Schubnell, J., et al., 2022a. Statistical characterization of stress concentrations along butt joint weld seams using deep neural networks. Appl. Sci. 12 (12), 6089. https://doi.org/10.3390/app12126089.

Braun, M., Kellner, L., Schreiber, S., Ehlers, S., 2022b. Prediction of fatigue failure in small-scale butt-welded joints with explainable machine learning. Procedia Struct. Integr. 38, 182–191. https://doi.org/10.1016/j.prostr.2022.03.019.

Cho, D., Nam, S., Cho, C., Lee, D., Jeong, E., Jeong, Y., et al., 2022. A new study on the fatigue properties of SA weld joints by considering the effects of welded bead shape. JMSE 10 (10), 1527. https://doi.org/10.3390/jmse10101527.

Fricke, W., 2015. Recent developments and future challenges in fatigue strength assessment of welded joints. Proc. Inst. Mech. Eng. Part C 229 (7), 1224–1239. https://doi.org/10.1177/0954406214550015. : Journal of Mechanical Engineering Science.

Harati, E., Karlsson, L., Svensson, L.E., Dalaei, K., 2015. The relative effects of residual stresses and weld toe geometry on fatigue life of weldments. Int. J. Fatigue 77, 160–165. https://doi.org/10.1016/j.ijfatigue.2015.03.023.

Hou, C., 2007. Fatigue analysis of welded joints with the aid of real three-dimensional weld toe geometry. Int. J. Fatigue 29 (4), 772–785. https://doi.org/10.1016/j.ijfatigue.2006.06.007.

Hultgren, G., Myrén, L., Barsoum, Z., Mansour, R., 2021. Digital scanning of welds and influence of sampling resolution on the predicted fatigue performance: modelling, experiment and simulation. Metals. (Basel) 11 (5), 822. https://doi.org/10.3390/met11050822.

Jung, M., Braun, M., Schubnell, J., Remes, H., 2024. Round robin study on the determination of weld geometry parameters - part A: analysis of a reference specimen. Weld World. https://doi.org/10.1007/s40194-024-01829-y.

Kažukauskas, E., Butkus, S., Jukna, V., Paipulas, D., Sirutkaitis, V., 2023. Scanning algorithm optimization for achieving low-roughness surfaces using ultrashort laser pulses: a comparative study. Materials. (Basel) 16 (7), 2788. https://doi.org/10.3390/ma16072788.

Lee, C.-H., Chang, K.-H., Jang, G.-C., Lee, C.-Y., 2009. Effect of weld geometry on the fatigue life of non-load-carrying fillet welded cruciform joints. Eng. Fail. Anal. 16 (3), 849–855. https://doi.org/10.1016/j.engfailanal.2008.07.004.

Magnus E.H.P. Good parameters for particle swarm optimization. Technical Report no. HL1001; 2010.

Merziger, G., 2013. Formeln + Hilfen Höhere Mathematik. [s.l.]. Binomi Verlag Barsinghausen.

Niederwanger, A., Warner, D.H., Lener, G., 2020. The utility of laser scanning welds for improving fatigue assessment. Int. J. Fatigue 140, 105810. https://doi.org/10.1016/j.ijfatigue.2020.105810.

Niraula, A., Remes, H., Lehto, P., 2023. Local weld geometry-based characterization of fatigue strength in laser-MAG hybrid welded joints. Weld World 67 (6), 1527–1544. https://doi.org/10.1007/s40194-023-01488-5.

Ottersböck, M.J., Leitner, M., Stoschka, M., Maurer, W., 2016. Effect of weld defects on the fatigue strength of ultra high-strength steels. Procedia Eng. 160, 214–222. https://doi.org/10.1016/j.proeng.2016.08.883.

Ottersböck, M.J., Leitner, M., Stoschka, M., 2021. Characterisation of actual weld geometry and stress concentration of butt welds exhibiting local undercuts. Eng. Struct. 240, 112266. https://doi.org/10.1016/j.engstruct.2021.112266.

Randić, M., Pavletić, D., Turkalj, G., 2019. Multiparametric investigation of welding techniques on toe radius of high strength steel at low-temperature levels using 3D-scanning techniques. Metals. (Basel) 9 (12), 1355. https://doi.org/10.3390/met9121355.

Renken, F., Schubnell, J., Jung, M., Braun, M., Remes, H., 2024. Round Robin study on the determination of weld geometry parameters – part B: analysis of welded specimen. Weld. World submitted for publication.

Renken, F., von, Bock und Polach RUF, Schubnell, J., Jung, M., Oswald, M., Rother, K., et al., 2021. An algorithm for statistical evaluation of weld toe geometries using laser triangulation. Int. J. Fatigue 149, 106293. https://doi.org/10.1016/j.ijfatigue.2021.106293.

Rohani Raftar, H., Ghanadi, M., Hultgren, G., Ahola, A., Barsoum, Z., Björk, T., 2024. Assessing local stresses in scanned fillet weld geometry using bagged decision trees. J. Constr. Steel. Res. 218, 108745. https://doi.org/10.1016/j.jcsr.2024.108745.

Schork, B., Kucharczyk, P., Madia, M., Zerbst, U., Hensel, J., Bernhard, J., et al., 2018. The effect of the local and global weld geometry as well as material defects on crack initiation and fatigue strength. Eng. Fract. Mech. 198, 103–122. https://doi.org/10.1016/j.engfracmech.2017.07.001.

Schork, B., Zerbst, U., Kiyak, Y., Kaffenberger, M., Madia, M., Oechsner, M., 2020. Effect of the parameters of weld toe geometry on the FAT class as obtained by means of fracture mechanics-based simulations. Weld World 64 (6), 925–936. https://doi.org/10.1007/s40194-020-00874-7.

Schubnell, J., Jung, M., Le, C.H., Farajian, M., Braun, M., Ehlers, S., et al., 2020. Influence of the optical measurement technique and evaluation approach on the determination of local weld geometry parameters for different weld types. Weld World 64 (2), 301–316. https://doi.org/10.1007/s40194-019-00830-0.

Schubnell, J., Konidena, S.K., Jung, M., Braun, M., Ehlers, S., Madia, M., et al., 2024. Approach for the probabilistic fatigue assessment of welded joints based on the local geometry of the weld seam. Fatigue Fract. Eng. Mater. Struct. 47 (1), 88–107. https://doi.org/10.1111/ffe.14170.

Shiozaki, T., Yamaguchi, N., Tamai, Y., Hiramoto, J., Ogawa, K., 2018. Effect of weld toe geometry on fatigue life of lap fillet welded ultra-high strength steel joints. Int. J. Fatigue 116, 409–420. https://doi.org/10.1016/j.ijfatigue.2018.06.050.

Shojai, S., Brömer, T., Ghafoori, E., Schaumann, P., 2024. Application of local fatigue approaches on corroded welded joints with consideration of weld geometry and residual stresses. Theor. Appl. Fracture Mech. 129, 104215. https://doi.org/10.1016/j.tafmec.2023.104215.

Stenberg, T., Barsoum, Z., Åstrand, E., Öberg, A.E., Schneider, C., Hedegård, J., 2017. Quality control and assurance in fabrication of welded structures subjected to fatigue loading. Weld World 61 (5), 1003–1015. https://doi.org/10.1007/s40194-017-0490-5.

Tsang, K.S., Pang, J.H.L., Hoh, H.J., 2018. Influence of weld toe radii on fatigue life prediction. MATEC Web Conf. 165, 22025. https://doi.org/10.1051/matecconf/201816522025.

Welding - Fusion-Welded Joints in Steel, Nickel, titanium and their alloys (beam welding excluded) - Quality levels for imperfections(ISO 5817); 2014.

Zerbst, U., Madia, M., Beier, H., 2017. Fatigue strength and life determination of weldments based on fracture mechanics. Procedia Struct. Integr. 7, 407–414. https://doi.org/10.1016/j.prostr.2017.11.106.